JOURNAL OF SPACECRAFT AND ROCKETS
Vol. 37, No. 1, January–February 2000

Aeroelastic Vehicle Dynamics of a Proposed Delta II 7920-10L Launch Vehicle

L. E. Ericsson*
Mountain View, California 94040
and
D. Pavish†
The Boeing Company, Huntington Beach, California 92647

A dynamic aeroelastic analysis has been performed using both experimental and computational-fluid-dynamics-derived surface pressure data to calculate modal damping for two Delta II 10-ft-diam payload fairing configurations. The maximum dynamic deflection was determined for a proposed 7920-10L stretch composite and the standard 7920-10 metal payload fairings. By the use of experimental pressure data and theoretical inviscid prediction, the maximum viscous loads could be defined in a worst-case analysis to determine the maximum possible response amplitude for the Delta II 7920-10C launch vehicle, describing single-degree-of-freedom oscillations in the first and second (lower-frequency) bending modes.

Nomenclature

A = axial force, coefficient $C_A = A/q_\infty(\pi d^2/4)$
$C_{m\dot{\theta}}$ = $\partial C_m/\partial(\dot{\theta}d/U_\infty)$
$C_{N\alpha}$ = $\partial C_N/\partial\alpha$
D_s = separation-induced aerodynamic damping derivative
d = maximum nose diameter
ℓ = vehicle length
M = Mach number
m = pitching moment, coefficient $C_m = m/q_\infty(\pi d^3/4)$
N = normal force, coefficient $C_N = N/q_\infty(\pi d^2/4)$
p = static pressure, coefficient $C_p = (p - p_\infty)/q_\infty$
q_∞ = dynamic pressure, $= \rho_\infty U_\infty^2/2$
U = velocity
x = axial coordinate
α = angle of attack
Δ = amplitude or increment
$\Delta^i C_N$ = separation-induced normal force
$\Delta\theta_N$ = oscillation amplitude at the nose tip
ζ_s = separation-induced aerodynamic damping as a fraction of critical damping
ζ_0 = structural damping as a fraction of critical damping
θ = pitch perturbation
θ_c = nose cone angle
ξ = dimensionless x coordinate, $(x - x_N)/d$ (Fig. 2)
ρ = air density
ϕ = mode deflection coordinate (Fig. 13)

Subscripts

crit = critical value
d = discontinuity (Fig. 15)
N = nose
s = flow separation
1, 2 = numbering subscripts
∞ = freestream conditions

Superscript

$-$ = integrated time-average value

Received 17 February 1999; revision received 17 September 1999; accepted for publication 21 September 1999.

*Engineering Consultant. Fellow AIAA.
†Principal Engineer, Aerodynamic Design, DELTA II and TITAN Programs, Boeing Aerospace.

Introduction

THE widespread present use of unmanned and unrecoverable launch vehicles has led to a need for review and update of aeroelastic analysis techniques developed in the 1960s. In most cases a conservative, simple analysis can ensure the structural integrity of the launch vehicle during its ascent through the critical transonic phase of its trajectory. The advantage of using a well-tested, reliable bus as first and second stages for a variety of arbitrary diameter, length, and shape payloads has led to renewed interest in hammerhead configurations. Early analytical and experimental investigations of hammerhead payload shrouds provided a degree of understanding of the associated aeroelastic problems.[1–5] In addition to the flow separation on the hammerhead boat tail, the flow separation occurring on the nose-cylinder shoulder of the payload can often be cause for concern.[6,7] Both types of flow separation can be present on the 10-ft-diam Delta payload fairing shroud.

Analytic Approach

A simple conservative analysis constitutes the first step in the determination of whether or not the structural integrety of the launch vehicle could be endangered during the ascent through the critical high subsonic and transonic speed regions. This is often the only analysis needed. If, however, this preliminary analysis shows that the dynamic, aeroelastic stability could be endangered, the next step is a more refined analysis with better-defined static aerodynamic loads. In some cases a third phase may be needed in which dynamic tests are performed, as in the case of the Saturn-Apollo, using either a fully elastic wind-tunnel model[8] or partial mode simulation.[9] However, in the overwhelming majority of investigations, only the first phase has been needed. It provides a fast, inexpensive means to ensure the structural integrity of the launch vehicle early in the design cycle. Where the initial analysis has indicated a possible aeroelastic problem, it also provides a quick method to check the efficiency of a proposed fix.

Cone-Cylinder Flow Separation

When investigating if the flow separation on the nose-cylinder shoulder of the payload can cause self-excited structural oscillations of the Delta launch vehicles for the two candidate payload fairings (Private communication of unpublished data for Delta 10S and Delta 10L Payload Shrouds, D. Pavish, Nov. 1993) (Fig. 1), it is useful to review past experience with respect to the potential for aeroelastic instability to be generated by the flow separation occurring on the cone-cylinder shoulder of a typical payload shroud.[6] Slender cone-cylinder forebodies usually do not cause the aerodynamicist or dynamicist any problems. However, there is one important exception. If a launch vehicle reaches moderate trim angles of

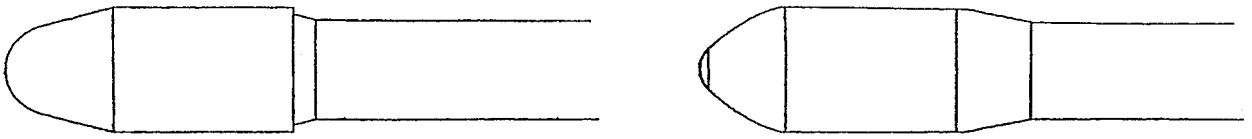

a) 10S standard payload shroud b) 10L composite payload shroud

Fig. 1 Delta II payload shroud configurations (Private communication, Pavish).

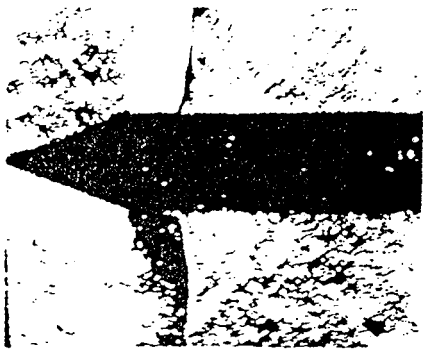

$M_\infty = 0.89, \alpha \sim 0°$

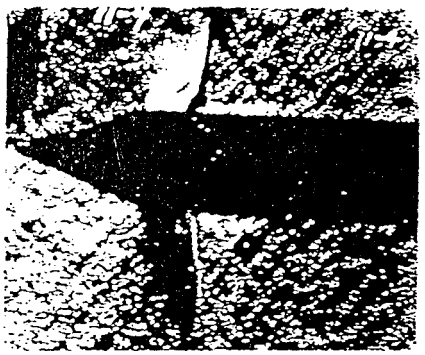

$M_\infty = 0.89, \alpha = 2°$

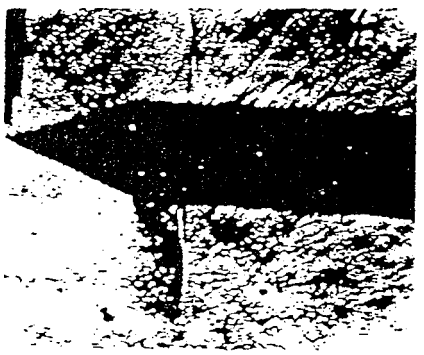

$M_\infty = 0.89, \alpha = 4°$

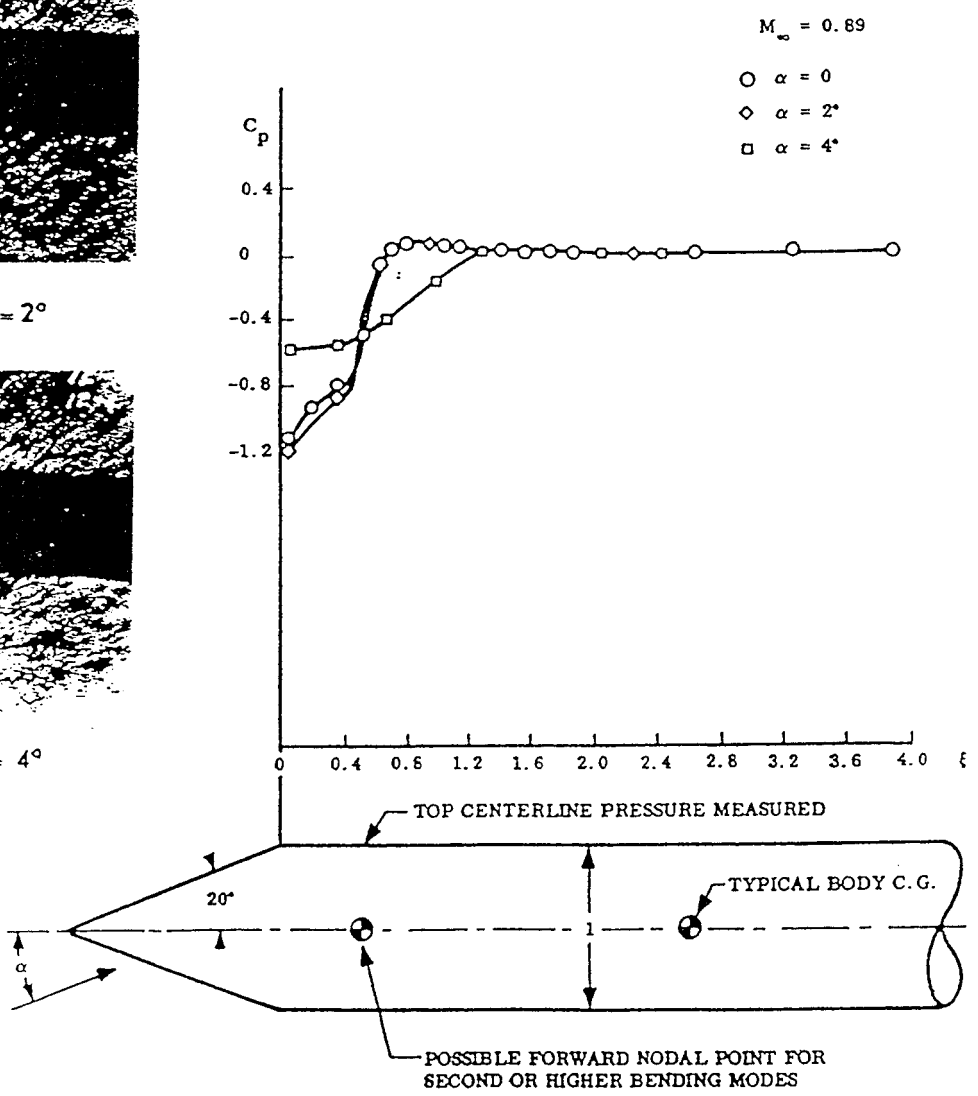

Fig. 2 Aerodynamic characteristics at $M_\infty = 0.89$ of a 20-deg cone-cylinder body with separated flow.[11]

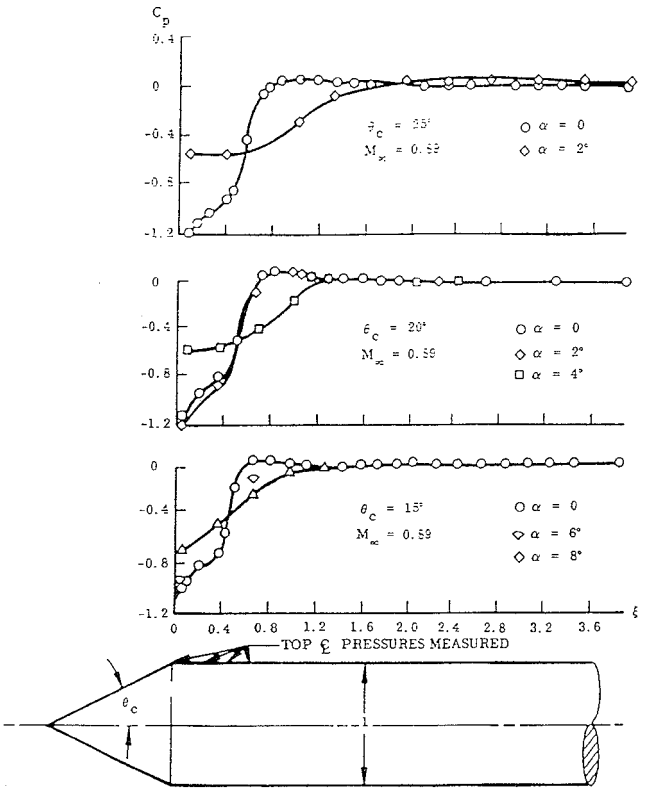

Fig. 3 Effect of cone angle on the occurrence of complete flow separation at $M_\infty = 0.89$ (Ref. 11).

attack (e.g., because of gusts) at high subsonic Mach numbers during its ascent, aeroelastic instability may result, even for payloads with cone half angles below 15 deg. The responsible flow phenomenon was discovered by Robertson and Chevalier.[10–12] They discussed, however, only the buffet input (i.e., the forcing function) and did not concern themselves with the other half of the problem as it presents itself to the aeroelastician, that is, they did not consider the vehicle response. The gross bending response of the vehicle is not critically dependent upon the buffet input per se, but rather on the aerodynamic undamping caused by the separated flow that produces the buffet input.[6] Reviewing the experimental data,[10] the following distinct characteristics are found. At high subsonic speeds a terminal shock appears downstream of the cone-cylinder shoulder, causing local boundary-layer separation[11] (Fig. 2). When the angle of attack exceeds a critical value, 2 deg $< \alpha_{crit} <$ 4 deg for $\theta_c = 20$ deg, the leeward side separation jumps forward to the cone-cylinder shoulder, causing a large discontinuous load change. The resulting force couple will not affect the rigid-body moment (aft c.g.) as much as the bending moment of an elastic mode with a forward node. As will be demonstrated, this discontinuous load change poses a serious aeroelastic problem. The sudden change to complete leeside flow separation occurs at a higher angle of attack the more slender the conical nose is[11] (Fig. 3). The test results[12] in Fig. 4 show how the flow oscillated between shock-induced and nose-induced separation in a large $M - \alpha$ region for a fixed model (within sting-stiffness limitations). For the 30-deg nose cone only the windward side had this alternating flow, whereas on the slender 15-deg cone cylinder only the leeward side had this type of alternating flow separation.

If the launch vehicle is at or near the critical angle of attack α_{crit}, it will experience the maximum aeroelastic response to this alternating flow separation. Figure 5 displays the separation-induced negative damping, or undamping, predicted for a Saturn booster[13] using

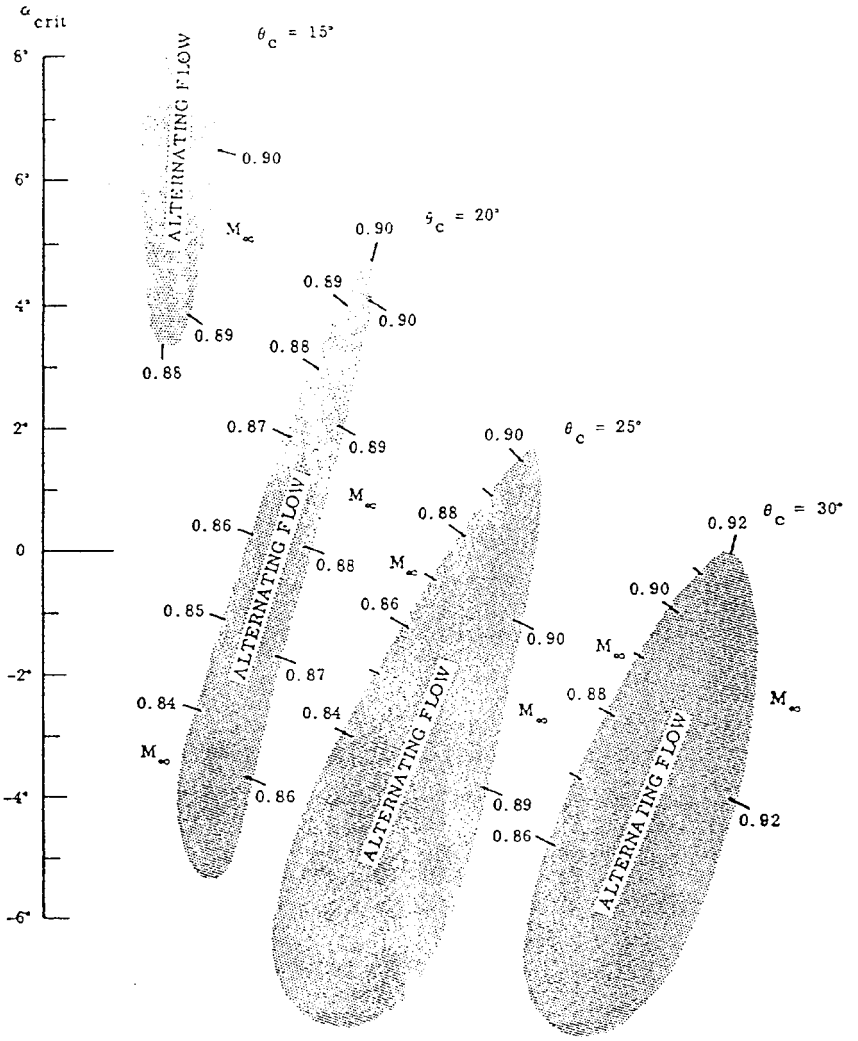

Fig. 4 Alpha-Mach-number regions for alternating flow separation and reattachment on cone-cylinder bodies with various cone angles.[12]

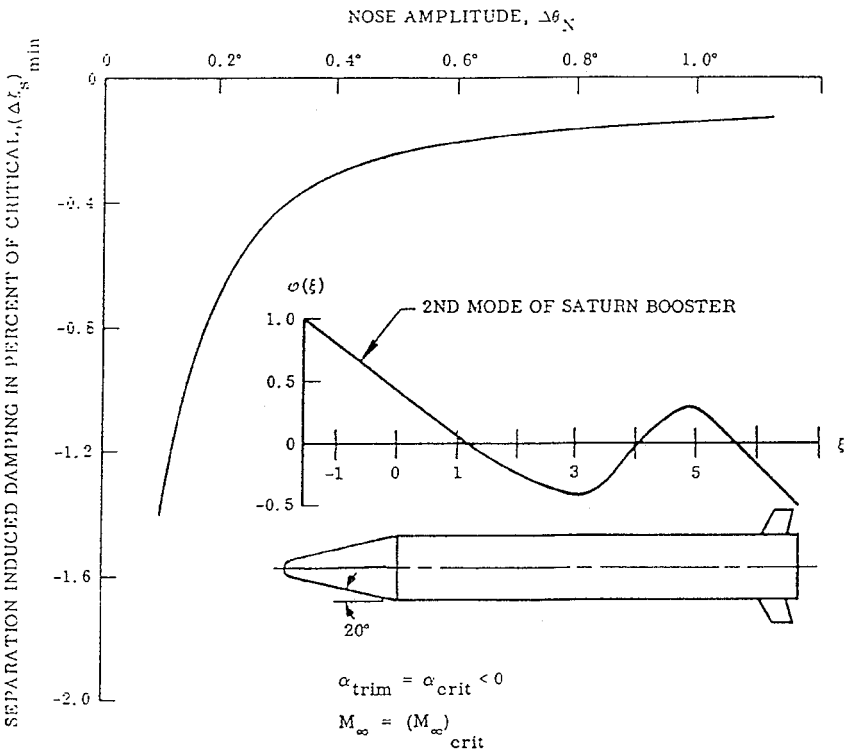

Fig. 5 Effect of complete flow separation on the damping of an elastic vehicle oscillating in its second bending mode at various amplitudes.[13]

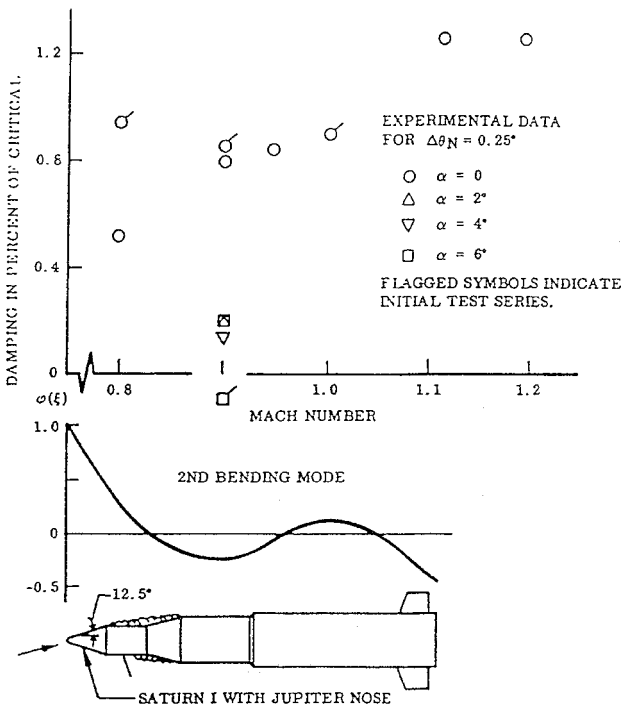

Fig. 6 Aerodynamic damping measured on an 8% scale elastic model of the Saturn I, block II launch vehicle with a Jupiter nose shroud.[14]

the experimental results for a 20-deg cone cylinder[11,12] (Fig. 2). A separation-induced negative damping of roughly 0.6% of critical damping is predicted for an oscillatory amplitude of $\Delta\theta_N = 0.25$ deg at the nose tip. Tests with a Saturn I elastic model[14] gave even larger separation-induced negative damping at $\alpha \geq 2$ deg and $M = 0.9$ (Fig. 6), most likely because of the presence of the downstream flare, which generates an adverse pressure gradient in addition to that generated aft of the cone-cylinder shoulder. For the Delta standard 10-ft-diam payload shroud (Fig. 1a), these cone-cylinder results are

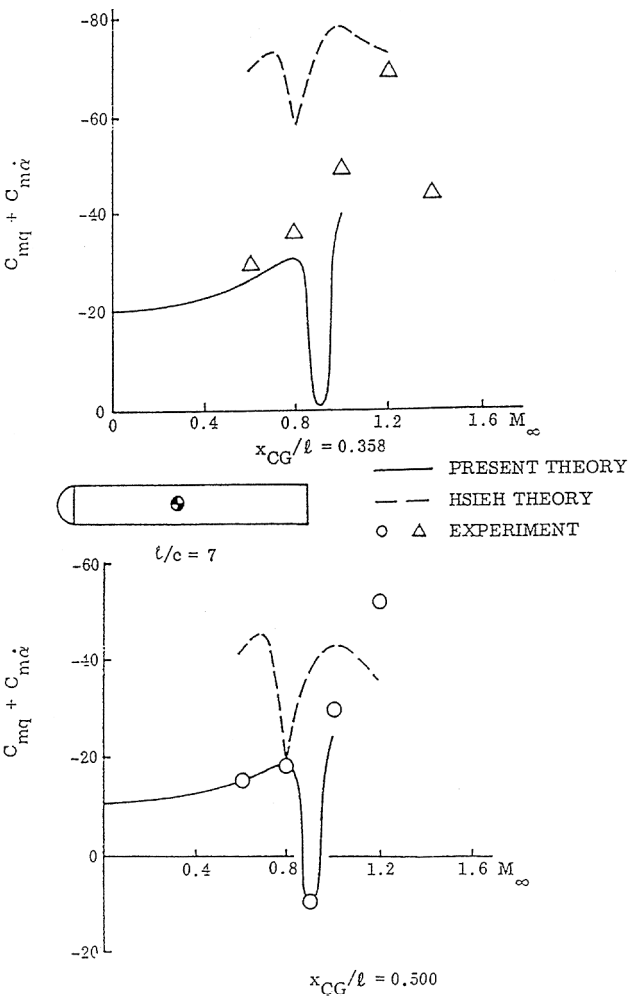

Fig. 7 Comparison between predicted and measured pitch damping of a hemisphere-cylinder body at $\alpha = 0$ (Ref. 16).

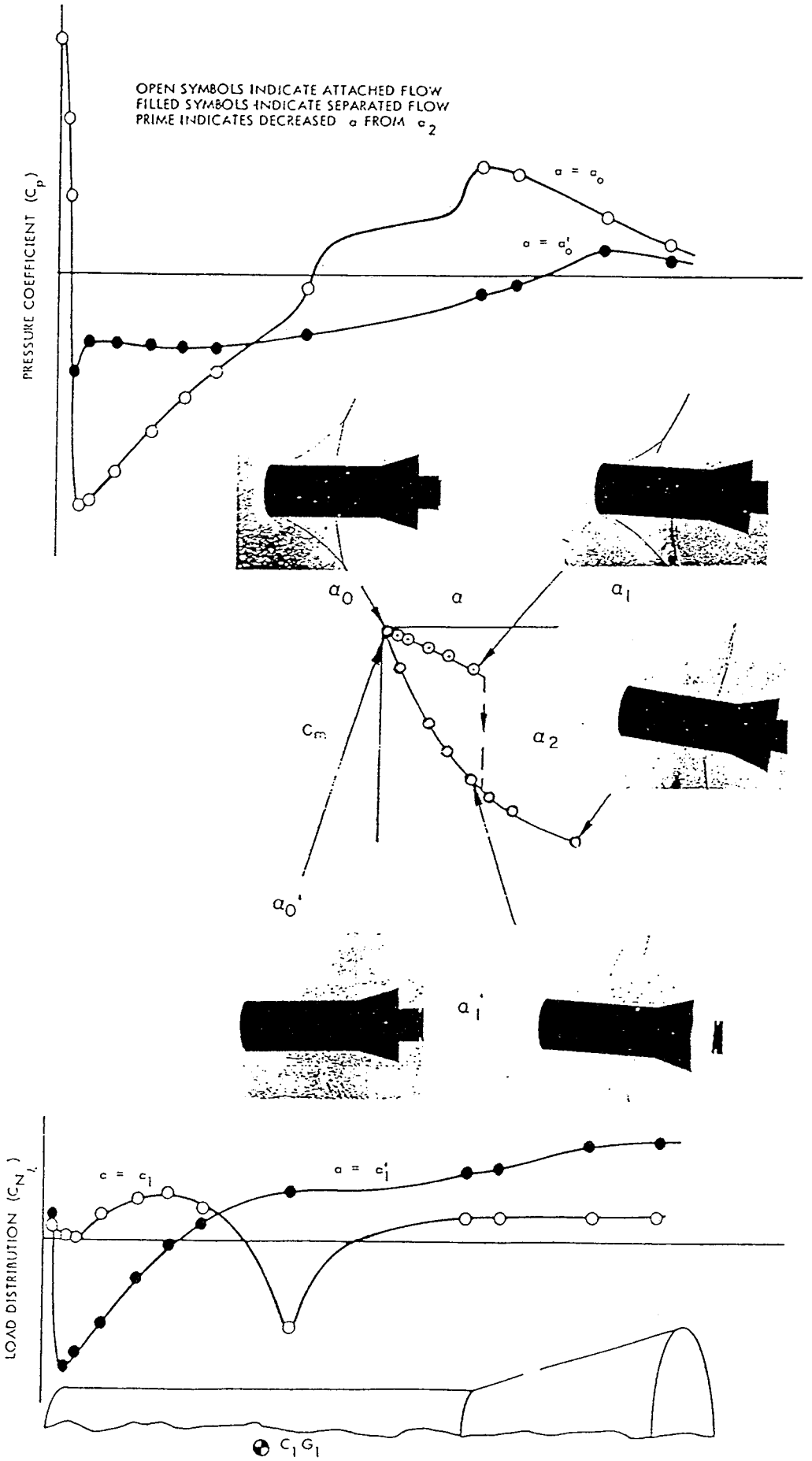

Fig. 8 Effect of global nose-induced and local retarded shock-induced flow separations on pressure and load distributions over a blunt-nose cylinder-flare body at $M_\infty \approx 1.00$ (Ref. 19).

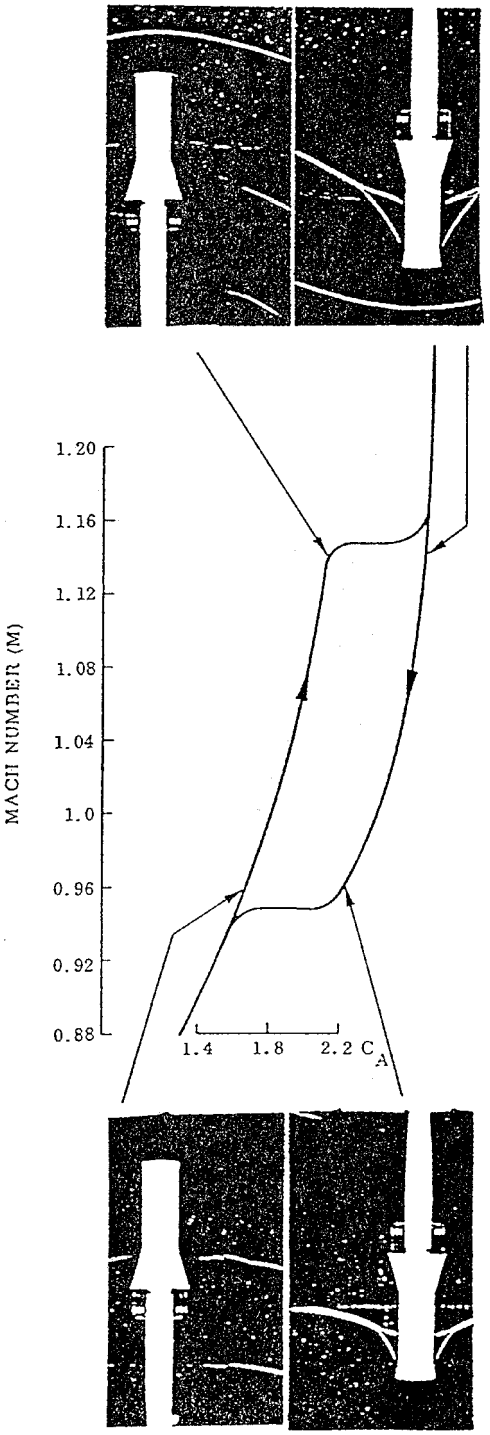

Fig. 9 Mach-number hysteresis at $\alpha = 0$ for flow separation on blunt-nose cylinder-flare body.[19]

of direct interest. It will be shown that similar separation-induced effects are also experienced by the Haack nose-cylinder shroud design (Fig. 1b).

A hemisphere-cylinder experiences nose-induced flow separation at zero angle of attack at high subsonic speeds. The negative damping generated by this flow separation on a hemisphere-cylinder body, observed in rigid-body experiments,[15] could be predicted[16] by applying the analysis of Ref. 4 to the rigid bending mode, using static experimental data as an input (Fig. 7). In contrast, a purely theoretical method[17] could not predict the experimentally observed loss of pitch damping at $M = 0.9$. As in the case of the cone-cylinder geometry discussed earlier (Fig. 6), the presence of a downstream flare promotes nose-induced flow separation. The difference is of quantitative rather than qualitative character. Thus, the experimental results for the Polaris reentry body[18,19] in Fig. 8 can be used to illustrate the discontinuous flow separation characteristics expected for the Delta shroud geometries (Fig. 1). In this case a discontinuous change from retarded shock-induced to nose-induced leeside flow separation occurs at $|\alpha| = \alpha_{crit} > 0$, similar to the change occurring on the cone cylinder in Fig. 2, where 2 deg $< \alpha_{crit} <$ 4 deg. The dual pressure and normal-force distributions shown in Fig. 8 could be obtained[18,19] because of the Mach-number hysteresis shown in Fig. 9. In the Mach-number range $0.9 < M < 1.16$, the flow separation at $\alpha = 0$ was of the shock-induced, retarded type if the Mach-number region was entered from the supersonic side, but was of the nose-induced type if the region was entered from the subsonic side. The experimental results in Fig. 8 were obtained by starting with the shock-induced flow separation at $\alpha = 0$, obtained by decreasing the Mach number from $M_\infty > 1.16$ to 1.00 (Fig. 9). When the angle of attack was increased beyond a critical value, the nose-induced, global separation was the only type that could exist unless the Mach number was increased above $M_\infty = 1.16$. Figure 8 illustrates the type of force couple that is generated in the case of the cone cylinder (Fig. 2).

Figure 10 shows that a large undamping effect is generated on the Polaris reentry body[18,19] by the sudden nose-induced flow separation, occurring when the amplitude $\Delta\theta$ of the oscillations around $\alpha = 0$ exceeds $\Delta\theta = |\alpha_{crit}|$. For oscillations around $\alpha = \alpha_{crit}$, the undamping effect would have been much larger, going to infinity as $\Delta\theta$ goes to zero, as in the case of the cone-cylinder geometry in Fig. 5. Because the nose amplitude $\Delta\theta_N$ that the structure of an elastic vehicle can withstand without failure usually is only a fraction of a degree, the discontinuous nature of the separation-induced aerodynamics is of much more concern for elastic than for rigid-body vehicle dynamics.

If an aeroelastic analysis of the Delta launch vehicle would indicate that the proposed shroud designs (Fig. 1) could cause separation-induced effects with the potential to endanger the structural integrity of the vehicle, a design change would be needed. The most feasible, and often the only possible, fix is to change the shroud geometry, thereby affecting the source of the problem, i.e., the sudden flow separation occurring on the payload shroud. The predictions made in Fig. 5 for the Saturn booster were obtained using experimental results[11,12] for the 20-deg cone-cylinder geometry (Fig. 3). The actual geometry was not conical but biconical, consisting of a 25-deg cone followed by a 12.5-deg conical frustum. Later tests showed this geometry to be devoid of the sudden nose-induced flow separation that plagued the simple conical nose geometry[6] (Fig. 11). The first shoulder or cusp between the 25-deg and 12.5-deg conical frustums causes the boundary layer to separate ahead of the cone-cylinder shoulder, and the reattaching boundary layer is strong enough to negotiate the cone-cylinder shoulder without separating.[20] This beneficial effect of preseparation of the boundary layer also has been observed on blunt nose shapes.[6]

Hammerhead Flow Separation

A hammerhead payload has by definition a larger maximum diameter than the adjacent booster and is, therefore, inevitably associated with some form of boat tail, which usually experiences flow separation. At high subsonic speeds the flow separation is of the shock-induced variety, exemplified by the Able IV payload[21] (Fig. 12). The flow on the leeward side experiences shock-induced flow separation, and negative lift is induced, which, because of the associated time lag effect, has a much larger impact on the dynamic aeroelastic characteristics than the negative boat-tail lift generated in attached flow. This separation-induced negative lift was of considerable magnitude on the shallow boat tail, causing undamped oscillations of the second bending mode.[2] Later analysis using computational fluid dynamics methods has given similar results.[22] This flow separation on the boat tail was in all probability the cause of the structural failure observed in flight. As the main source of the large adverse aeroelastic effect of the Able IV payload is the large movement of the shock-induced boundary-layer separation, one fix is to eliminate this degree of freedom, e.g., by fixing separation to take place at the start of the boat tail., e.g., by requiring the designer to use a boat-tail angle of 30 deg or more[23] or by using a skirt, as in the

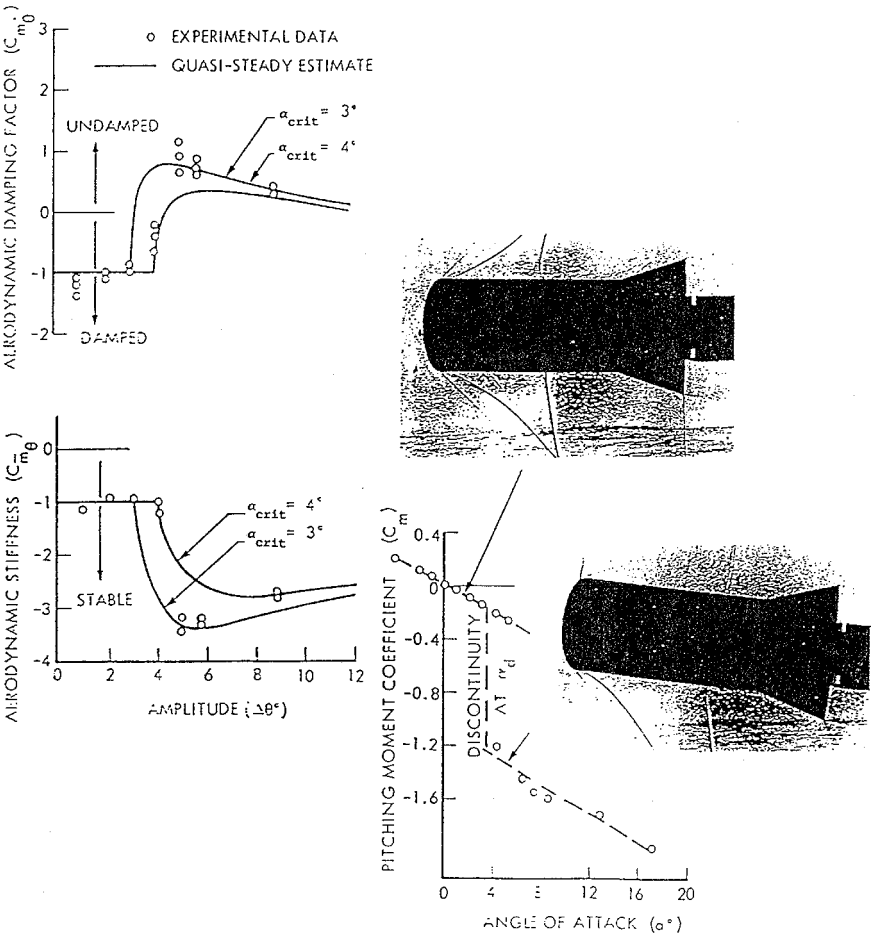

Fig. 10 Dynamic effects of separation-induced pitching moment discontinuities at transonic Mach numbers.[9]

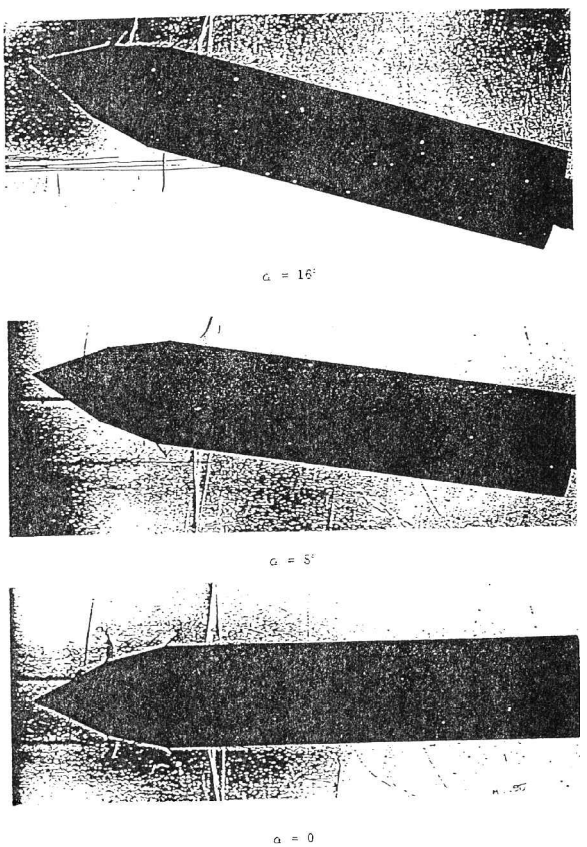

Fig. 11 Shadowgraphs of the flow over the Saturn IB SA-203 launch vehicle with a biconic nose geometry at $M = 0.9$ and $\alpha = 0, 8$, and 16 deg (Ref. 20).

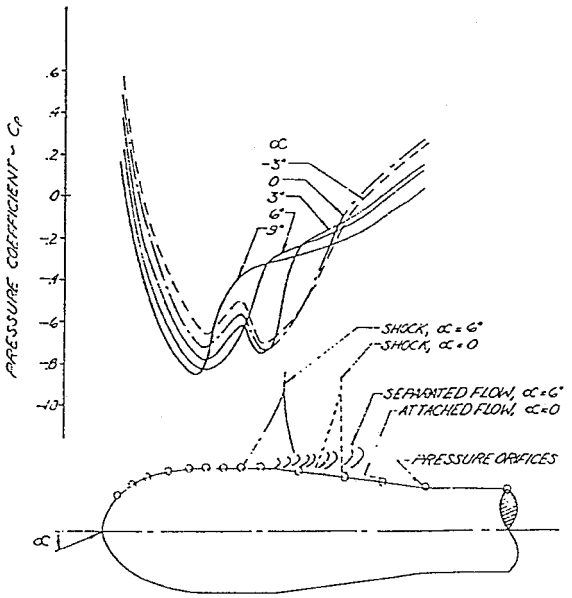

Fig. 12 Pressure distribution over the Atlas Able IV payload shroud at $M = 0.96$ (Ref. 21).

case of the Delta 10S shroud design (Fig. 1a). This increased steepness of the boat tail will, with a few exceptions,[7,24,25] eliminate the aeroelastic problem.

Aeroelastic Analysis

The dynamics of the elastic vehicle are analyzed for single-degree-of-freedom oscillations of the low-frequency bending modes[26] (Fig. 13). The key information needed in such an analysis is a description of the loads generated by the occurring flow separation.

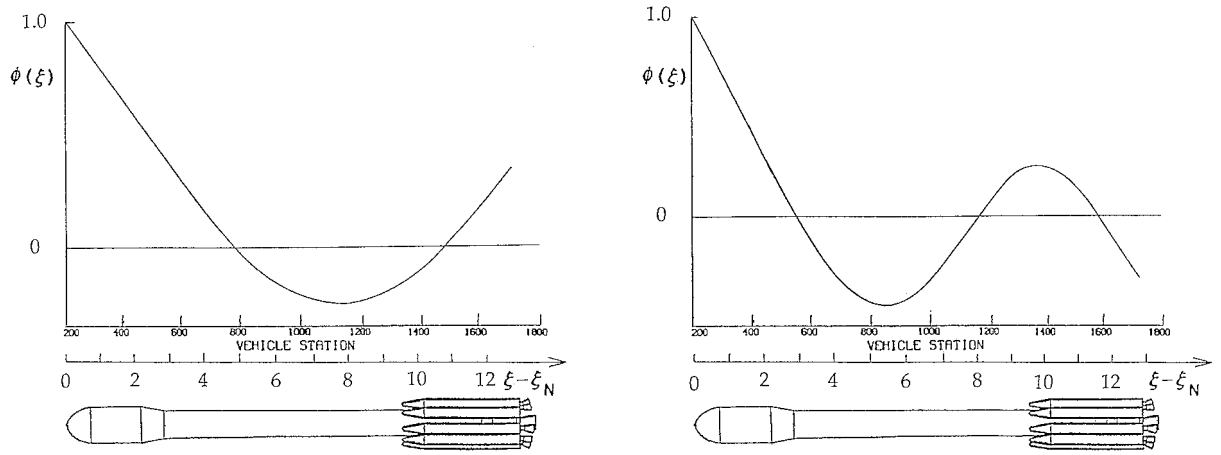

a) First bending mode b) Second bending mode

Fig. 13 Bending mode shapes for Delta launch vehicle with 10L payload fairing.[26]

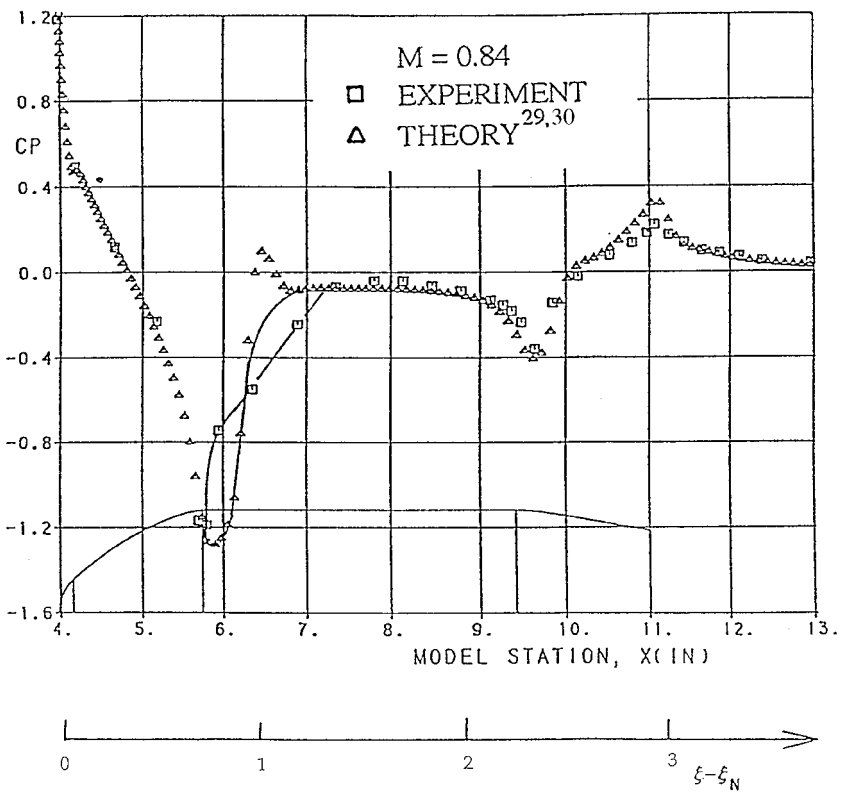

Fig. 14 Pressure distribution over Delta 10L payload shroud at $\alpha = 3$ deg and $M = 0.80$ (Ref. 26). Experimental results are from private communication, Pavish.

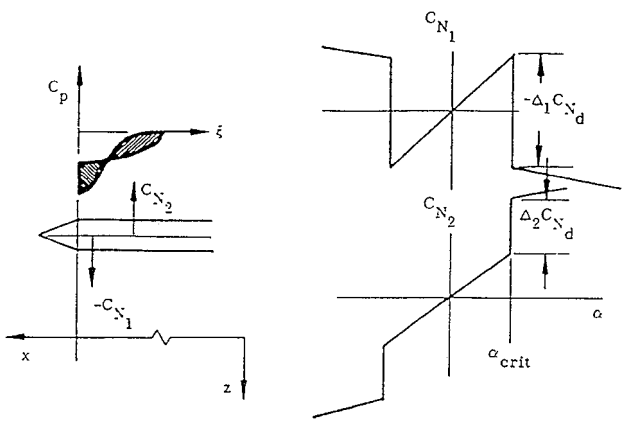

Fig. 15 Separation-induced discontinuous load changes on cone-cylinder bodies.[26]

These loads are determined as the difference between the loads measured in wind-tunnel tests and the theoretical loading existing in inviscid flow. In past analyses of cone-cylinder geometries,[6,27] the inviscid loads were determined by a shock-expansion method.[28] In the present case they are obtained by solving the Euler equations[29,30] (Fig. 14). The force couple in Fig. 14 is similar to that in Figs. 2 and 3 for the cone-cylinder geometry. Using the definitions in Fig. 15, the analysis in Ref. 26 gave the results shown in derivative form in Fig. 16. In percent of critical the undamping for the first bending mode (Fig. 16a) is as shown in Fig. 17. The oscillation amplitude $\Delta\theta_N = 0.28$ deg, resulting at $M = 0.80$ for the available 1.5% structural damping, was well within the structural capability.

In Fig. 18 the experimental pressure distribution (Private communication, Pavish) is shown at $M = 0.90$ for the top centerline at $\alpha = 0$ and 3 deg. In this case there is no change on the top side from retarded shock-induced to nose-induced flow separation. The shocks were placed as close to the extreme positions as the density of the pressure instrumentation allowed. In this manner the experimental results in

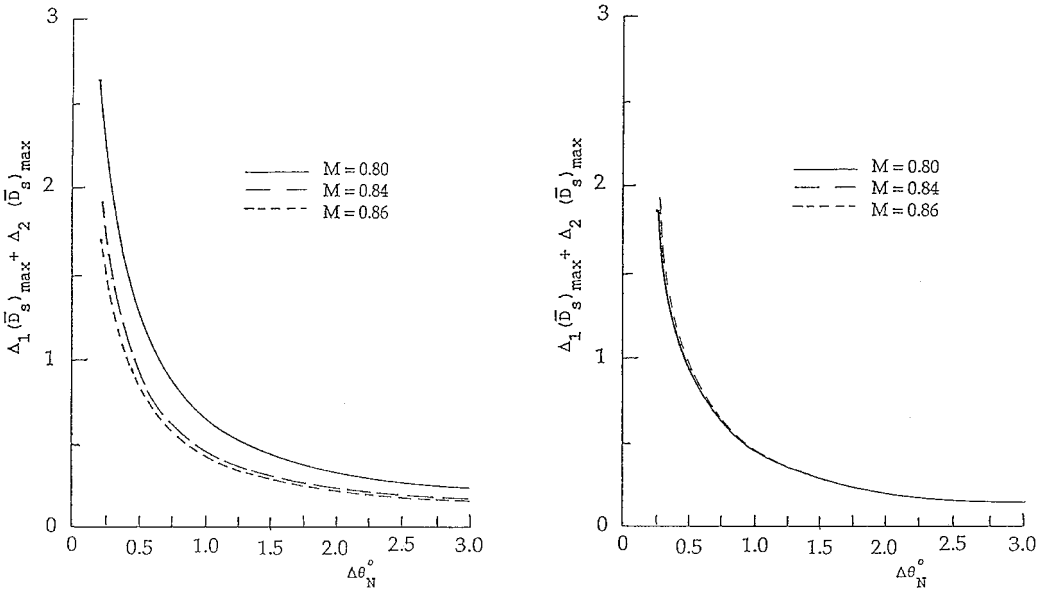

a) First bending mode b) Second bending mode

Fig. 16 Separation-induced undamping on the Delta launch vehicle with 10L payload fairing.[26]

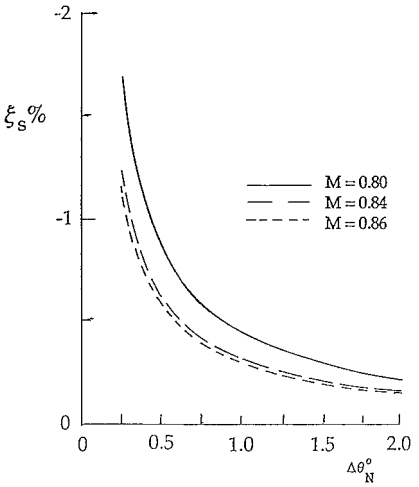

Fig. 17 Separation-induced undamping in percent of critical damping for the first bending mode of the Delta launch vehicle with the 10L payload shroud.[26]

Fig. 18 for $\alpha = 0$ and 3 deg at $M = 0.90$ were used to define the maximum adverse cylinder load $\Delta^i C_N = -0.073$, corresponding to $\Delta^i C_{N\alpha} = -1.40$. At $\alpha = 0$ the slope could be of larger magnitude, but it is unlikely to exceed the peak value $\Delta^i C_{N\alpha} = -1.9$ obtained for the 20-deg cone cylinder.[27] Using this larger magnitude of the separation-induced force derivative $\Delta^i C_{N\alpha} = -1.9$, together with a representative mean value for the range of shock positions assumed in Fig. 18, gives the separation-induced undamping $\zeta_s = -0.010$ for the first bending mode at the flight conditions existing at $M = 0.90$. Thus, even this high estimate of the maximum possible magnitude of the separation-induced undamping can be handled by the available structural damping $\zeta_0 = 0.015$. This maximum possible undamping can only exist at $\alpha = 0$, where both top and bottom sides generate undamping. At $\alpha = 3$ deg, for example, the undamping would be of lesser magnitude, as only the top, leeward side generates undamping in this case.

Using the extreme shock positions in Fig. 18 to evaluate also the separation-induced loads on the boat tail gives $\Delta^i C_{N\alpha} = -1.26$, yielding $\zeta_s = -0.0054$. If one adds this conservative estimate to the equally conservative estimate of the contribution from the cylindrical portion at $\zeta_s = -0.014$, one would get a combined separation-induced undamping that exceeds the available 1.5% structural damping. However, one has to consider that this large undamping could occur only if $\alpha = 0$ and that the extreme shock positions used in Fig. 18 to obtain $\Delta^i C_N$, and thereby $\Delta^i C_{N\alpha}$, will produce estimates of the maximum possible separation-induced undamping that are highly unrealistic. The probability that the placing of the orifices used for the pressure measurements would be such that the shock-induced flow separation just was missed is extremely small. That this unlikely event would occur simultaneously on the cylinder and the boat tail is too remote to merit consideration.

The shock-induced separation on the boat tail of the Delta 10L payload shroud (Fig. 18) is much milder than that occurring on the Able IV payload (Fig. 12). The reason for this is that the upstream flow separation on the cylinder will cause a preseparation effect similar to that for the biconic nose cylinder in Fig. 11. As the Mach number is increased from $M = 0.90$ (Fig. 18) to 0.95 (Fig. 12) or higher, the two shock-induced flow separations on the Delta 10L payload shroud (Fig. 18) will merge and occur on the boat tail. From Fig. 12 one obtains $\Delta^i C_N = -0.060$ for $\alpha = 3$ deg, giving a force derivative $\Delta^i C_{N\alpha} = -1.18$, which should be compared with the overestimate $\Delta^i C_{N\alpha} = -1.26$ obtained from Fig. 18. Using the latter, very conservative value gives $\zeta_s = -0.012$ for the flight conditions at $M = 0.95$, well below the magnitude of the available structural damping $\zeta_0 = 0.015$.

The crossflow effects on the boundary-layer buildup on the leeward side of the payload shroud are likely to be much larger on the Able IV with its long, elliptic nose than on the Delta 10L payload shroud. Thus, the estimate obtained by using the Able IV results (Fig. 12) should be very conservative. It is therefore reassuring to find that even in that case the available structural damping ($\zeta_0 = 0.015$) will be sufficient to ensure the structural integrity of the Delta 10L launch vehicle. As the crossflow effect on the boundary layer is expected to be larger for the Able IV than for the Delta 10L payload shroud, the results for $\alpha = -3$ deg in Fig. 12 should also give a very conservative estimate of the effect of the shock-induced flow separation on the windward side. The data in Fig. 12 indicate that the effect is small. Thus, the estimate of the undamping effect at $\alpha = 0$ and $M = 0.90$ of the shock-induced flow separation on the cylindrical portion of the Delta 10L payload shroud, discussed earlier, is completely unrealistic. It should be much closer to $\zeta_s = -0.007$ than to $\zeta_s = -0.014$, in which case even adding the overestimated contribution $\zeta_s = -0.0054$ from the boat tail (Fig. 18) would not exceed the magnitude of the available structural damping $\zeta_0 = 0.015$.

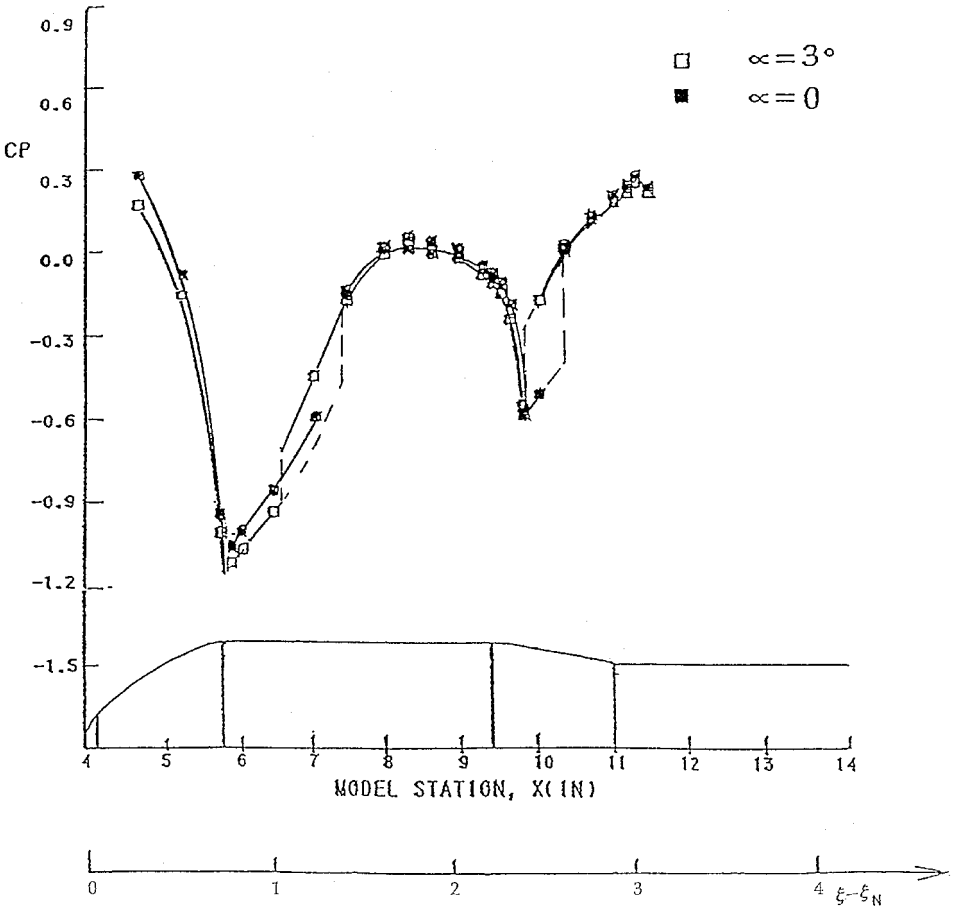

Fig. 18 Experimental top-side pressure distribution over Delta 10L payload shroud at $M = 0.90$ (Ref. 26).

Conclusions

A worst-case analysis of the aeroelastic stability of a proposed Delta II 7920-10L launch vehicle, using experimental viscous and theoretical inviscid static pressures to determine the maximum possible aerodynamic undamping, showed that the available 1.5% structural damping will ensure structural integrity through the critical subsonic-transonic speed region of the vehicle ascent.

References

[1]Ericsson, L. E., Woods, P., and Chavez, J. N., "A Mechanism for Self-Excited Oscillations on Hammerhead and Other Blunt-Nose Missiles," *Proceedings of the 6th Symposium on Ballistic Missile and Aerospace Technology*, Vol. 4, Aerospace Corp., San Bernadino, CA, 1961, pp. 69–88.

[2]Woods, P., and Ericsson, L. E., "Aeroelastic Considerations in a Slender, Blunt-Nose, Multistage Rocket," *Aerospace Engineering*, Vol. 21, No. 5, 1962, pp. 42–51.

[3]Rainey, A. G., "Progress on the Launch-Vehicle Buffeting Problem," *Journal of Spacecraft and Rockets*, Vol. 2, No. 3, 1965, pp. 289–299.

[4]Ericsson, L. E., and Reding, J. P., "Analysis of Flow Separation Effects on the Dynamics of a Large Space Booster," *Journal of Spacecraft and Rockets*, Vol. 2, No. 4, 1965, pp. 481–490.

[5]Ericsson, L. E., and Reding, J. P., "Fluid Dynamics of Unsteady Separated Flow. Part I-Bodies of Revolution," *Progress in Aerospace Sciences*, Vol. 23, No. 1, 1986, pp. 1–84.

[6]Ericsson, L. E., "Aeroelastic Instability Caused by Slender Payloads," *Journal of Spacecraft and Rockets*, Vol. 4, No. 1, 1967, pp. 65–73.

[7]Reding, J. P., and Ericsson, L. E., "Hammerhead and Nose-Cylinder-Flare Aeroelastic Stability Revisited," *Journal of Spacecraft and Rockets*, Vol. 32, No. 1, 1995, pp. 55–59.

[8]Rainey, G., "Progress on the Launch Vehicle Buffeting Problem," *Proceedings of the 5th Annual Structures and Materials Conference of the American Institute of Aeronautics and Astronautics*, AIAA, New York, 1964, pp. 163–177.

[9]Cole, H., Jr., Robinson, R., and Gambucci, B., "Buffeting Response of the Apollo Partial Mode Model at Subsonic and Supersonic Mach Numbers," NASA TN-D 2669, Feb. 1965.

[10]Robertson, J. E., "Unsteady Pressure Phenomena for Ballistic Missile Shapes at Transonic Speeds," AIAA Paper 64-3, Jan. 1963.

[11]Robertson, J. E., and Chevalier, H. L., "Characteristics of Steady-State Pressures on the Cylindrical Portion of Cone-Cylinder Bodies at Transoniac Speeds," Arnold Engineering Development Center, AEDC TDR-63-104, Tullahoma, TN, Aug. 1963.

[12]Chevalier, H. L., and Robertson, J. E., "Pressure Fluctuations Resulting from Alternating Flow Separation and Attachment at Transonic Speeds," Arnold Engineering Development Center, AEDC TDR-63-204, Tullahoma, TN, Nov. 1963.

[13]Ericsson, L. E., and French, N. J., "The Aeroelastic Characteristics of the Saturn 1B SA-203 Launch Vehicle," NASA CR-76563, April 1966.

[14]Hanson, P. W., and Dogget, R. V., Jr., "Aerodynamic Damping and Buffet Response of an Aeroelastic Model of the Saturn I Block II Launch Vehicle," NASA TND-2713, March 1965.

[15]Shadow, T. O., and Paulk, R. A., "Dynamic Stability Characteristics of Bluff Bodies of Revolution at Transonic Mach Numbers," Arnold Engineering Development Center, AEDC-TR-72-110, Tullahoma, TN, Aug. 1972.

[16]Ericsson, L. E., and Reding, J. P., "Approximate Slender Vehicle Dynamics at All Speeds," *Proceedings of the Eleventh Navy Symposium on Aeroballistics*, Vol. 1, Naval Sea Systems Command, Trevose, PA, 1978, pp. I-87–I-113.

[17]Hsieh, T., "Unsteady Transonic Flow over Blunt and Pointed Bodies of Revolution," AIAA Paper 78-211, Jan. 1978.

[18]Ericsson, L. E., and Reding, J. P., "Dynamics of Separated Flow," NASA CR-76912, Dec. 1965.

[19]Ericsson, L. E., "Separated Flow Effects on the Static and Dynamic Stability of Blunt-Nosed Cylinder-Flare Bodies," NASA CR-76919, Dec. 1965.

[20]Ericsson, L. E., French, N. J., and Guenther, R. A., "The Aeroelastic Characteristics of the Saturn IB Launch Vehicle with Biconic Payload Shroud," Lockheed Missiles and Space Co., LMSC M-37-65-1, Sunnyvale, CA, June 1967.

[21]Graham, F. J., and Butler, C. B., "Static Pressure Distribution on a 0.07 Scale Aerodynamic Model of the Atlas-Able IV at Free-Stream Mach Numbers from 0.50 to 1.60," Arnold Engineering Development Center, AEDC TN-60-128, Tullahoma, TN, July 1960.

[22]Azevedo, J. L. F., "Aeroelastic Analysis of Hammerhead Payloads," AIAA Paper 88-2307, April 1988.

[23]*NASA Space Vehicle Design Criteria, Vol. II: Structures, Part B: Loads*

and Structural Dynamics, Chap. 3: Launch and Exit, Sec. I: Buffeting, NASA SP-8001, May 1964.

[24]Reding, J. P., and Ericsson, L. E., "Effect of Aeroelastic Considerations on Seasat-A Payload Shroud Design," *Journal of Spacecraft and Rockets*, Vol. 18, No. 3, 1981, pp. 241–247.

[25]Ericsson, L. E., "Hammerhead Wake Effects on Elastic Vehicle Dynamics," *Journal of Spacecraft and Rockets*, Vol. 34, No. 2, 1997, pp. 145–151.

[26]Ericsson, L. E., "Delta 10L Composite Fairing Unsteady Aerodynamic Analysis," Nielsen Engineering and Research, NEAR TR 474, Contract 93664129 for McDonnell Douglas Aerospace, Huntington Beach, CA, March 1994.

[27]Ericsson, L. E., "Loads Induced by Terminal-Shock-Boundary-Layer Interaction on Cone-Cylinder Bodies," *Journal of Spacecraft and Rockets*, Vol. 7, No. 9, 1970, pp. 1106–1112.

[28]Syvertson, C. A., and Dennis, D. H., "A Second-Order Shock-Expansion Method Applicable to Bodies of Revolution Near Zero Lift," NACA Rept. 1328, 1957.

[29]Jameson, A., Wolfgang, S., and Turkel, E., "Numerical Solution of the Euler Equations by Finite Volume Methods Using Runge Kutta Time Stepping Schemes," AIAA Paper 81-1259, June 1981.

[30]Shmilovich, A., "On Transonic Flow Computations About Airfoils, Axisymmetric Projectiles and Nacelles in Free Air and in Wind Tunnels," Douglas Aircraft Co., MCD Rept. J3852, Huntington Beach, CA, Oct. 1985.

R. M. Cummings
Associate Editor